PL-GEODESICS ON *PL*-CONTINUOUS PARTIAL MESHES

Oscar E. Ruiz, Carlos A. Cadavid M.

Laboratory of CAD / CAM / CG
EAFIT University, A.A.(P.O. Box) 3300
Medellin
COLOMBIA
e-mail: {oruiz,ccadavid}@eafit.edu.co

ABSTRACT

Geometric characteristics of 2-manifolds embedded in $\boldsymbol{R}^3$ space have been analyzed from the point of view of differential geometry and topology. In the past, results relevant to these areas have been found for $\boldsymbol{C}^\infty$ curves and surfaces. However, current scientific, industrial, entertainment and medical applications, and availability of more powerful point sampling systems, press for characterization of discrete counterparts for the continuous properties and characteristics evaluated previously in $\boldsymbol{C}^\infty$ curves and surfaces. Recent works have presented estimation methods for properties such as the principal and rotated quadrics of point sampled surfaces. The present article uses the findings of previous investigations to propose and implement a method for evaluation of planarity of surfaces. It is based on: (i) Estimation of a $\boldsymbol{C}^0$ partial mesh fitting sets of planar or grid sample points. (ii) Evaluation of the piecewise - linear (PL) version of families of geodesic curves on the mesh. (iii) Diagnostic of the property of planarity based on the behavior of the families of geodesic curves. The present work can be applied in the area of design and manufacturing of products based on sheet materials, such as apparel, metal stamping, thin structures, etc.

Keywords: discrete differential geometry, PL geodesics, partial meshing, geometric algorithms, shape reconstruction.

Glossary

$\boldsymbol{M}$	2-manifold in $\boldsymbol{R}^3$ ($\boldsymbol{C}^\infty$ or $\boldsymbol{C}^0$ or ***PL***, with / without boundary).
PL	Piecewise Linear.
$\boldsymbol{(u, v)}$	pixel coordinates in range picture space.
$\boldsymbol{a, b}$	limits of parameterization interval for a path in $\boldsymbol{R}^3$.
$\boldsymbol{p, q, p_i, q_j}$	points in $\boldsymbol{R}^3$. Vertices of triangular facets.
$\boldsymbol{\alpha(t)}$	parameterized path in $\boldsymbol{R}^3$.
$\boldsymbol{v_i}$	directing vector of the i-th section of a PL path. Coincident with constant velocity of the PL geodesic on the i-th facet.
$\lambda, \boldsymbol{t}$	parameter in the parametric form of a section in a PL path.
face	domain on 2-manifold $\boldsymbol{M}$ in $\boldsymbol{R}^3$ whose boundary is a disjoint union of simple closed paths.
facet	triangle in $\boldsymbol{R}^3$.
$\boldsymbol{f_i}$	facet.
$\boldsymbol{n}$, $\boldsymbol{n_i}$, $\boldsymbol{n_h}$	normal vectors.
δ	distance between two points on $\boldsymbol{M}$, below which they belong to the same facet.
shell	synonymous with a "connected PL 2-manifold with boundary", and with "partial mesh".
$\boldsymbol{n_h}$	normal vector. Parameter of the Householder transformation.
$\boldsymbol{K}$	simplicial complex in $\boldsymbol{R}^3$.
$\lvert\boldsymbol{K}\rvert$	polyhedron defined by the simplicial complex $\boldsymbol{K}$.
$\boldsymbol{S}$	digitization point set in $\boldsymbol{R}^3$.

1. INTRODUCTION

Traditionally, differential geometry has developed results for $\boldsymbol{C}^\infty$ curves and surfaces in $\boldsymbol{R}^3$. In this direction, many important results have been found and applied in other areas of shape analysis, such as differential topology. It is the case of geometric characterization of critical points, n-handles, etc., as a resource to diagnose the topological characteristics

of manifolds ([Fomen97]). Currently, popularization of data capture from shapes by using range images, contact devices, magnetic resonance, ultrasound, tomographies, etc., makes available large sets of point data. This popularity of point sets has stressed the needs for estimating differential geometry properties of surfaces and curves from which only a partial, discrete and noisy sample is available. The parameters estimated include Gauss and mean curvatures, normal planes, Frenet frames, bilinear and trilinear surface approximations, principal frames, etc. Statistical methods applied to the data in some cases facilitate the estimation of such properties. In others, quantification of the effects of the statistical tools applied is not a trivial task, and therefore they are applied in an empirical way. Such is the case of filtering. Efforts in the direction of controlled application of both pre-processing and meshing tools render satisfactory results. Specific works are addressed in the literature review.

Authors have reported that estimation of discrete differential geometry properties from meshes is more accurate and efficient than estimation from (treated) point data ([McIvo97]). Following this experience, this investigation anchors the estimation of interesting constructions (in this case geodesic curves) on the consistent topological representation of partial meshes, rather than on the point data (raw or treated). Partial B-reps have been incorporated in [Ruiz99, Ruiz00] to manage partially sampled objects (for example, from range images). This representation naturally supports the estimation of discrete geodesics on partial meshes.

Geodesics are of interest since they are effective tools to assess the flatness of a surface. Informally, a surface is "flat" if geodesics which are parallel at some neighborhood remain parallel when prolonged (they keep the angle and distance between them). As a consequence, orthogonal families of geodesics remain orthogonal. Wrapped surfaces such as cylinders or cones are flat since geodesics drawn on them keep always their distance and angle to each other. Once a surface is assessed as flat, the geodesics themselves render the procedure to map it to $\boldsymbol{R}^2$ with no deformation. Therefore, flatness assessment is useful when material must be accounted for in the production of inherently thin goods: clothes, metal panels, structures, etc.

In this paper, section 2 discusses relevant literature. Section 3 presents the methodology for partial mesh construction. Section 4 proposes the calculation of piecewise - linear geodesics based on the partial B-rep of section 3. Section 5 displays the results and section 6 concludes the paper.

2. LITERATURE REVIEW

For a panoramic review of shape reconstruction see [Varad97]. In the present review only focused topics will be addressed.

Data Acquisition: Range imaging records a depth field in grid patterns corresponding to pixel arrays. A range picture is represented as a rectangular array with coordinates (u, v). If pixel (u, v) actually corresponds to a piece of the object calibrated (which is not a shadow or background) it has associated the coordinates (x, y, z) of the surface point $\boldsymbol{p}$ hit by the ray passing through the pixel, as well as the vector (v_x, v_y, v_z) describing the ray ([Turk94, Curle96, Neuge97]). The grid data so obtained contains implicit neighborhood information that facilitates topology reconstruction. However, such reconstruction is not trivial because the picture may register surface regions that are distant to each other, and there is no direct information as to whether they are actually different objects or self occluding parts of the same one.

Topology Recovery: In the surveyed literature Alpha Shapes ([Edels94]) and Marching Cubes ([Loren87]) are used as engines for recovering topology information ([Guo97, Neuge97]). In this article an alternative scheme will be followed as regular watertight closed B-Rep models ([Mantÿ88]) do not serve partial surface reconstruction. Therefore, an extended B-Rep structure is devised here to record absence of surface and existence of borders on some parts of the recognized surface or partial mask (possibly with holes as in a carnival mask) in which no completion should be made .

Some authors have tried to directly assess differential geometry properties with sampled point data ([McIvo97]). Their conclusion is that facetting information renders more precise and computationally effective results. DigitLAB [Ruiz99, Ruiz00] is reported as an environment with statistical, filtering and topology tools for construction of partial and complete B-reps and facetting information.

Regarding the carrier geometries of the partial B-rep, this investigation uses very simple geometries such as 3 and 4 - vertex facets. The last ones are of course not flat in general, but can be easily subdivided into triangles. These primitives have been found sufficient to support a correct topology. The issue of generalized parametric smoothing will not be addressed here, but may be browsed in [Grimm95].

The calculation of differential geometry properties of objects (geodesics, tangent planes, etc) on planar faceted representations present two aspects

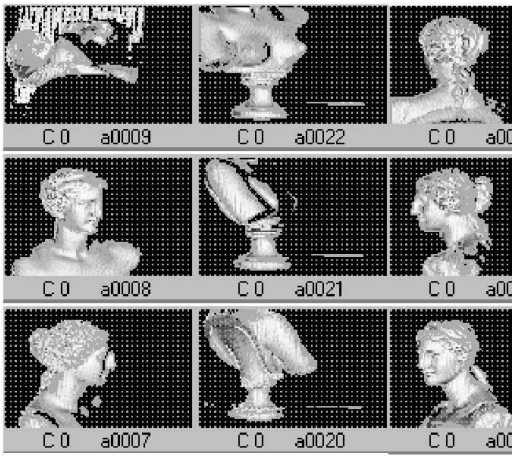

Aphrodite data set as processed by registration software (SCULPTOR, Fraunhofer IGD).
Figure 1.

(see following sections): (i) Representation of topological information into a piecewise - linear 2-manifold with boundary (implemented with a partial B-rep), so that its geometrical properties can be calculated. (ii) Translation and application of continuos version of differential geometry formulae to a discrete C^0 surface.

3. RECOVERY OF A 2-DIMENSIONAL MANIFOLD WITH BOUNDARY

The first step in calculating discrete geodesics is to determine the surface or manifold in which they are embedded. The following definitions assist in such a task ([Dodso91, Fomen97]):

2-dimensional manifold with boundary in $\boldsymbol{R^3}$: $\boldsymbol{M} \subset \boldsymbol{R^3}$ is *a smooth (or C^∞) 2-manifold with boundary* if $\forall\, \boldsymbol{x} \in \boldsymbol{M}$, $\exists$ open $\boldsymbol{U} \subset \boldsymbol{R^3}$ with $\boldsymbol{x} \in \boldsymbol{U}$ and $\boldsymbol{U} \cap$ M is diffeomorphic to an open set of $\boldsymbol{R^2_+}$ ($\boldsymbol{R^2_+} = \{(x, y) \mid y \geq 0\}$) ([Guill74]). If one replaces *diffeomorphic* by *homeomorphic* in this definition, $\boldsymbol{M}$ would be a *topological (or C^0) 2-manifold with boundary*.

Piecewise - linear Manifold with Boundary. If $\boldsymbol{M} \subset \boldsymbol{R^3}$ is a topological 2- manifold with boundary such that $\boldsymbol{M} = |\boldsymbol{K}|$ where $\boldsymbol{K}$ is a simplicial complex in $\boldsymbol{R^3}$, we say that $\boldsymbol{M}$ is a *PL 2-manifold with boundary* or (if connected) a *shell*. Manifolds without boundary are a special case of those with boundary.

Fig. 1 shows a series of calibrated and registered range pictures in the SCULPTOR software (Fraunhofer Institute for Computer Graphics). Each pixel (u, v) in a picture contains the information of the (x, y, z) coordinates of the object surface that are touched by the view ray passing by the pixel (along with other data not discussed here).

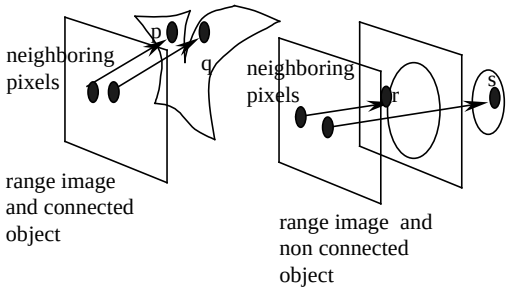

Variation in the topological location of neighboring pixels in the range image.
Figure 2.

SCULPTOR makes the necessary calculations to present the data as would be produced by rays impacting the object. From the calibration process, the black areas are considered either as background or shaded in the image, and therefore the range picture presents no evidence of object existence in the those pixels (u, v).

The immediate goal when having range pictures is to recover neighboring information present in them. However, care must be exercised since neighboring pixels in the range image (Fig. 2) may correspond to points that are too distant on one surface or, lie on different surfaces or different objects. This consideration leads to two conclusions: (i) The topological data chosen must be flexible enough to express separate shells on each picture, each one incomplete and possibly with holes. (ii) The algorithms to recognize and extract those shells must account for propagated neighborhoods based on a transitive proximity relation, rather than a direct, simple Euclidean criteria. Based on this concept, points $\boldsymbol{p}$ and $\boldsymbol{q}$ will enter the same shell (left case), while points $\boldsymbol{r}$ and $\boldsymbol{s}$ will never share a shell.

3.1 Spatial Relations for Shell Building

The definition of the basic relations between points are discussed next. Let (u_0, v_0), (u_1, v_1) and (u_2, v_2) be three pixel vertices, representing p_0, p_1, p_2 points on the object surface. The goal is to calculate a partition on the set of pixels, defined so that its equivalence relation is the belonging to the same topological shell apparent from the range picture. The following relations are formalized:

image_unit_triangle: three pixel vertices (u_0, v_0), (u_1, v_1), (u_2, v_2) form an ***image_unit_triangle*** if: $|u_i - u_j| \leq 1$ and $|v_i - v_j| \leq 1$, $0 \leq i, j \leq 2$ (i.e. they are immediate neighbors in the grid).

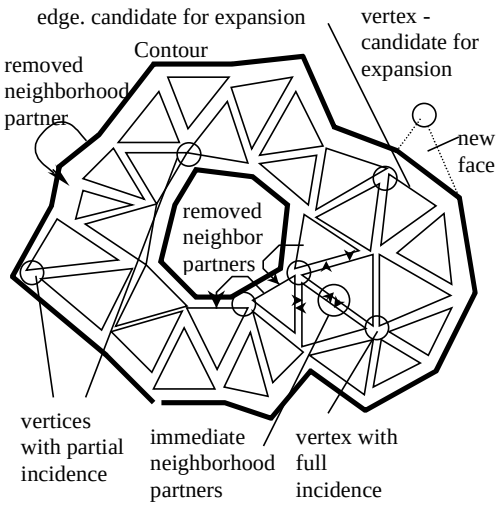

Summary of partial B-rep (boundary representation) for meshes.
Figure 3

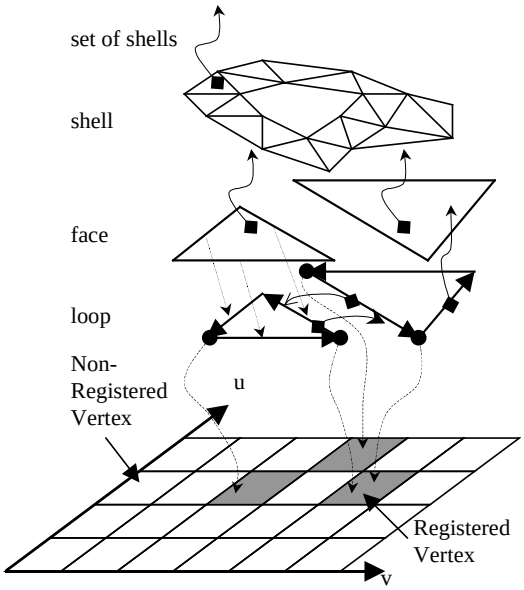

Relation between B-Rep and range image.
Figure 4

object_triangle: three points p_0, p_1, p_2 form a triangle on the object surface (***object_triangle***) if: (i) ***image_unit_triangle***$((u_0, v_0), (u_1, v_1), (u_2, v_2))$ and (ii) $\| p_i - p_j \| \le \delta$, ($0 \le i, j \le 2$).

This means, the three vertices are immediate neighbors on the grid and represent samples closer than δ (see Glossary) on the object.

transitive_neighbors: two points p, q on the object are ***transitive_neighbors*** if $\exists$ ***path(p , q)***=[$p=p_0$, p_1 ,...,$p_n=q$] sequence of points p_i such that ***object_triangle***(p_i , p_{i+1} , r) ($0 \le i \le n-1$, for some vertex r). Therefore, $\| p_i - p_{i+1} \| \le \delta$ ($0 \le i \le n-1$). This means, they are part of a chain of neighboring triangles, and ***path(p , q)*** is a path with traversal steps no larger than δ. Informally, there is a trail of object triangles that contains p and q.

Notice that ***transitive_neighbors( )*** is an equivalence relation (i.e. it is symmetric, reflexive, transitive). Therefore it induces a partition on the point set S (see Glossary). The equivalence classes are the point sets S_i of the separate shells registered in the range picture.

$$S = \cup S_i , S_i \cap S_j = \phi , i \neq j \qquad (1)$$

No two shells may share a vertex (otherwise they would be one). In the implementation, isolated surface points are not considered, and they are purged, as each of them would form a zero size, isolated triangle. Notice that the definitions above allow shells with holes, as required.

3.2 Partial Mesh Boundary Representation

Figs. 3 and 4 display a sketch of the data organization implemented to represent partial meshes. Observe that the neighborhood information is fundamental in this application, since properties of surfaces (curvatures, geodesics, etc) must be calculated based on sets of neighboring faces. Fig. 5 shows a macro algorithm that builds a partial mesh from range picture information. This algorithm uses the equivalence relations just discussed, to extend a seed mesh via its internal and external contours until it includes all possible "transitive neighbors".

4. GEODESIC CONSTRUCTION ON A PL 2-MANIFOLD WITH BOUNDARY

The following definitions are a needed introduction on the calculation of geodesics: (i) Geodesics on a smooth 2-manifold with boundary M : A geodesic is a smooth path $\alpha : (a , b) \rightarrow M \subset R^3$ whose acceleration $\alpha''(t)$ is always normal to M ([O'Neil66, Stoke89]). In the following, M will denote a PL 2-manifold with boundary in R^3.

(ii) Piecewise - linear (PL) path. A path $\alpha: [a,b] \rightarrow M$ is PL if there is a partition $a=t_0 < t_1 < .. < t_{n-1} < t_n = b$ such that on each subinterval $[t_i, t_{i+1}]$, α takes the form

$$\begin{aligned} \alpha : [t_i, t_{i+1}] &\rightarrow f_i \\ t &\rightarrow \alpha(t_i) + (t - t_i) v_i \end{aligned} \qquad (2)$$

where f_i is the facet of M, crossed by the i-th stage of the PL path and v_i is a vector on the plane containing f_i. Notice that it has been implicitly assumed that the numbering of the facets coincides with the

```
function range_pict_to_shells(rp:range_picture ):
                                        shell : B-rep
  shell = find_isolated_triangle( rp )
  contours_to_expand = {contour(shell) }
  while contours_to_expand
    contour = first(contours_to_expand )
    mesh_is_expandable = TRUE
    e = first_expandable_edge( contour, rp )
    done_contour = FALSE
    while (e)
      v=vertex_to_expand(e, rp)
      if expansion_splits_contour( contour, e, v)
          [c1,c2]=split_contour(contour, e, v)
          contours_to_expand=
            contours_to_expand + {c1,c2}
          e = NULL ;
      else
          t=make_new_triangle( e, v)
          shell = shell + {t}
          update(contour(shell), t)
          e = next_expandable_edge(e, contour, rp)
          if (not( e ))
            done_contour = TRUE ;
          end if
    end while
    if ( done_contour )
      contours_to_expand =
          contours_to_expand – {contour }
    end if
    contour = first( contours_to_expand )
  end while
end function
```

Macro-Algorithm for construcion of the 2-manifold $\boldsymbol{M}$
Figure 5.

numbering of the stages in the PL path. Therefore, if the PL path crosses the same facet more than once, such facet will reappear with different index each time.

(iii) Acceleration of a PL path. The acceleration of α (a PL path) is defined by

$\alpha''(t) = 0$ if $t \neq a, t_1, \ldots, t_n, b$
$\alpha''(t) = v_i - v_{i-1}$ if $t = t_i$ for some i in $1..n-1$

(iv) normal vector $\boldsymbol{n(p)}$ at each point $\boldsymbol{p}$ of $\boldsymbol{M}$: Under the assumption that $\boldsymbol{M}$ is orientable, let $\boldsymbol{n_i}$ be the unit vector normal to facet $\boldsymbol{f_i}$ induced by a fixed orientation on $\boldsymbol{M}$. We define:

$n(p) = n_i$, if $p \in Int(f_i)$
$n(p) = n_i + n_j$, if $p \in Int(f_i \cap f_j)$ and $f_i \cap f_j \neq \phi$.
$n(p) = n_{i1} + n_{i2} + \ldots + n_{ir}$, if $p \in f_{i1} \cap f_{i2} \ldots \cap f_{ir}$.
and $f_{i1}, f_{i2}, \ldots, f_{ir}$ are all the facets that have p as common vertex.

In addition to the above definition, the normalization of $\boldsymbol{n(p)}$ is required. In what follows, $\boldsymbol{n(p)}$ denotes a unit vector.

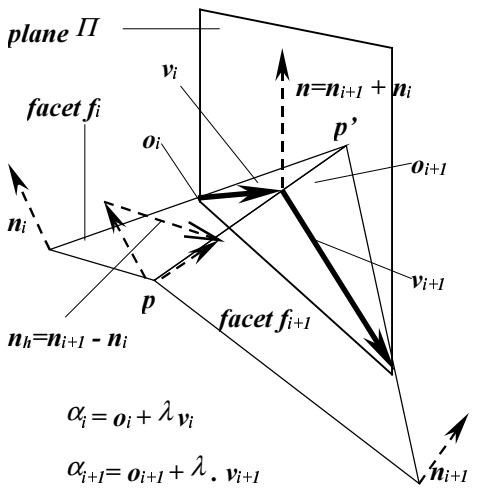

Generic discrete geodesics on facets $\boldsymbol{f_i}$ and $\boldsymbol{f_{i+1}}$.
Figure 6.

(v) PL Geodesic. A PL path $\alpha: [a,b] \rightarrow M$ is a PL-geodesic iff $\alpha''(t)$ is parallel to $n(\alpha(t))$ for each t in interval (a,b).

In consequence: (a) For each facet f_i, α has constant velocity vector on each connected component of the set $\alpha^{-1}(Int(f_i))$. This means that on each facet the geodesic does not zig-zag or changes its velocity magnitude. It may cross several times the same facet. (b) A portion of the geodesic on facet f_i can be expressed as $\alpha_i(\lambda) = o_i + \lambda . v_i$, where o_i is the point on the boundary of facet f_i, where α enters the facet. v_i is the constant velocity of the geodesic on facet f_i.

In this subsection we give a method to construct a PL geodesic, starting at a given point on the interior of a facet $Int(f_0)$, and with a given initial velocity vector v_0, contained in the plane of the facet f_0. The case in which the geodesic eventually hits a vertex or coincides with an edge of the B-rep is discussed separately.

4.1 Generic PL Geodesic Stage

The present discussion addresses the generic case in which the geodesic only touches facet boundaries in two non - vertex points. Fig. 6 shows the case in which the ***i-th*** stage of the geodesic is known, and the goal is to compute the stage ***i+1***. The following notation is used:

- n_i , n_{i+1}: unit vectors, normal to facets f_i and f_{i+1}. Their precise definition appears in section 4, entry (iv).
- $\alpha_i(\lambda) = o_i + \lambda . v_i$: parametric form of the geodesic on facet f_i (known).
- $\alpha_{i+1}(\lambda) = o_{i+1} + \lambda . v_{i+1}$: parametric form of the

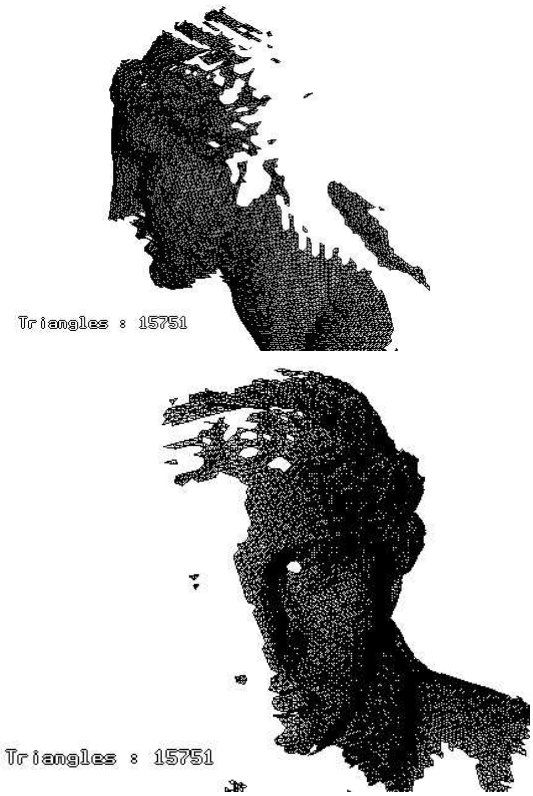

"Aphrodite" data set. Two views of a partial shell from a range picture.
Figure 7.

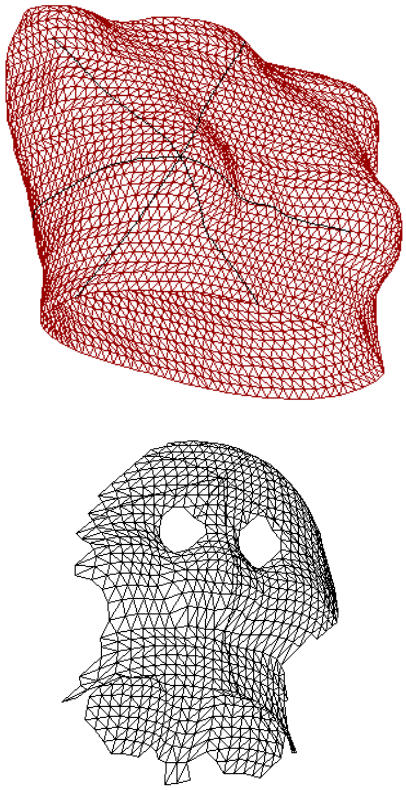

Star pattern geodesics on facetted partial b-reps. Data sets *woman torso* and *teddy bear*.
Figure 8.

geodesic on facet f_{i+1} (to determine).

p, p' : end points of the edge between facets f_i and f_{i+1}.

$n = n_{i+1} + n_i$: approximate normal vector on the limit between facets f_i and f_{i+1} (edge $p\,p'$).

Formula 3 allows to calculate o_{i+1}, the origin of α_{i+1}:

$$\begin{bmatrix} v_i & p - p' \end{bmatrix} \begin{bmatrix} \lambda \\ \rho \end{bmatrix} = \begin{bmatrix} p - o_i \end{bmatrix} \qquad (3)$$

where

$o_{i+1} = o_i + \lambda \, . \, v_i$, and $o_{i+1} = \rho.p + (1-\rho).p'$ $(0 \le \rho \le 1)$.

Formula (3) has less unknowns than equations. This characteristic obeys to the fact that in this case vector v_i is constrained to be on facet f_i. To actually solve the system one introduces a slack variable β, which takes value 0 whenever v_i is contained in the plane of f_i (as in the present conditions).

Once o_{i+1}, the initial point of the geodesic α_{i+1} in the facet f_{i+1} is known, v_{i+1} must be determined. The condition for geodesics forces the relation:

$$(v_{i+1} - v_i) \times (n_i + n_{i+1}) = 0 \qquad (4)$$

A geometrical argument can be used to find v_{i+1}: It must be noticed that v_{i+1} is the mirror image of v_i about the plane that is normal to the vector $n \times v_i$ ($n = n_{i+1} + n_i$ with n_i , n_{i+1} unit vectors). The vector v_{i+1} can be found by applying the Householder transformation ([Golub94]), that mirrors a vector about a plane with a given unit normal n_h . In this case:

$$n_h = n \times (n \times v_i) \,/\, \| \, n \times (n \times v_i) \, \| \qquad (5)$$

The Householder transformation with parameter n_h, applied to $(-v_i)$ would be:

$$v_{i+1} = H_{nh}(-v_i) = (I - 2\, n_h \; n_h^T)\,(-v_i) \qquad (6)$$

Where v_{i+1}, v_i and n_h are column vectors, I is the 3x3 identity matrix, and all products are matrix ones. As a by-product of condition (4), in this case the magnitude of the v_i and v_{i+1} vectors is the same. The Householder transformation indeed reflects this fact.

4.2 Vertex-crossing PL Geodesic Stage

The calculation of geodesics is based on the normal vector to the surface. In the generic case, described before, such a normal is approximated by the summation of the two normals of incoming facets on

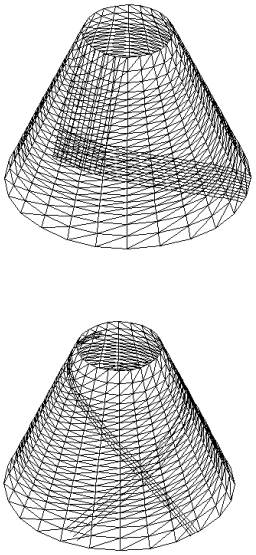

Orthogonal evenly spaced geodesics on a flat surface.
Figure 9.

the edge ***p-p'***. When the geodesic hits a vertex of the B-rep, determining a vector that behaves formally as the normal to the surface at that point is a complex task. Also, the facets that the geodesic traverses when leaving the vertex must be determined. This investigation attacked those exceptions by defining the vector normal to the PL manifold in a vertex as the normalized summation of the normals of the incident facets to that vertex $\boldsymbol{n}=\Sigma \boldsymbol{n}_i \;/\; \| \Sigma \boldsymbol{n}_i \|$. Observe that this approach does not ensure that the $\boldsymbol{v}_{i+1}$ vector leaving the vertex (applying Householder) would lie on any of the facets $\boldsymbol{f}_i$ incident on vertex $\boldsymbol{o}_{i+1}$. Therefore, one approximates the exit vector by: (1) Defining Π as the plane that contains $\boldsymbol{o}_{i+1}$ and vectors $\boldsymbol{n}$ and $\boldsymbol{v}_i$. (2) Determining the intersection between Π and the incoming facets to $\boldsymbol{o}_{i+1}$. This determines which facet is crossed by $\boldsymbol{v}_{i+1}$ when leaving the vertex $\boldsymbol{o}_{i+1}$. (3) Ensuring that the magnitude of $\boldsymbol{v}_{i+1}$ equals that of $\boldsymbol{v}_i$. In order to apply this approximation it is assumed that vertex $\boldsymbol{o}_{i+1}$ is a convex one. This ensures that (i) there will be exactly one exit facet containing $\boldsymbol{v}_{i+1}$ and, (ii) $\boldsymbol{n}=\Sigma \boldsymbol{n}_i \;/\; \| \Sigma \boldsymbol{n}_i \| \neq \boldsymbol{0}$.

5. RESULTS

Fig. 7 presents the reconstruction of the PL 2-manifold with boundary from range picture data for the *Aphrodite* data set. As requested, the proposed structure accommodates disjoint portions, different objects on the picture, and holes that may be present either because the original object has them, or because there is a dark region in the picture. Fig. 8. shows the results of star pattern geodesics on data sets "teddy bear" and "woman torso". The algorithm implemented works also in degenerate cases in which the geodesic hits a vertex or coincides with an edge in the extended B-rep representing the PL 2-manifold. In the case shown, the geodesics keep no particular relation among themselves. Initially orthogonal, evenly spaced geodesics, converge or grow apart as they develop, changing also their intersection angles. This is, of course, a consequence of the fact that the manifolds are intrinsically non-flat. In contrast, Fig. 9 presents a pattern of two families of geodesics. Within a family, these curves are evenly spaced, parallel to each other. They are perpendicular to the geodesics in the other family when they are born ($\boldsymbol{t=0}$ in parameter space). The goal is to test whether they keep such relations as they develop (parameter $\boldsymbol{t}$ grows). In effect, the crossing angles keep remarkably close to 90 degrees over all the intersections, and their distance (parallelism) is also kept.

Complexity of Algorithms Presented. The discrete geodesics algorithm has as pre-condition the availability of facet neighboring information, naturally available in the partial B-rep implemented. The geodesics algorithm proceeds by traversing the partial B-rep, passing from a facet to the neighbor until a "border" is found. That means, places where a facet has no neighbor via a particular edge. The B-rep construction algorithm (Fig. 5) costs $O((\boldsymbol{N.M})^3)$ where $\boldsymbol{N}$ and $\boldsymbol{M}$ are the number of pixels in horizontal and vertical directions in the range picture. Calculating each stage of the geodesic has constant cost. Since the geodesic could involve every facet, it might be executed $O((\boldsymbol{N.M})^2)$ times. This argument concludes that the partial B-rep or shell construction plus the geodesics calculation cost $O((\boldsymbol{N.M})^3)$ operations.

6. CONCLUSION

The algorithms presented for calculation of discrete or piecewise - linear geodesics could diverge because of numerical error and the approximations to the continuous counterparts. However, in the examples run they present extremely good numerical stability. In these conditions, they could be used to unroll the manifold, since the relative position of surface points in "geodesic" space is exactly replicated in $\boldsymbol{R}^2$. Therefore, surface point geodesic coordinates serve to map manifold points to $\boldsymbol{R}^2$, and with them all the B-rep structure just created. In the cases shown, material stock evaluation follows immediately, as well as hits on the manufacturing process. In the cases in which the deformation of the geodesic pattern indicates non-flatness of the surface, in the future, the deformation itself may be used as an estimator of the deviation between the manifold and its "nearest" flat image. This estimation allows the quantification of material

needed, and the effect of deformation processes such as thermoforming (for example in the manufacture of women underwear, metal sheet stamping, etc.).

ACKNOWLEDGMENTS

The authors wish to thank the economic support of the Deutscher Akademischer Austaushdienst (DAAD) for the internship of Assoc. Prof. Dr. Oscar Ruiz at Fraunhofer IGD's in 1999 and the Colombian Institute for Science and Technology (Colciencias) through grants FALCON-98 and 99. Assistants Miguel Granados and Eliana Vasquez have helped with implementations on MATLAB and C++ on AutoCAD ARX.

REFERENCES

[Curle69] Curless, B., Levoy, M., A volumetric Method for Building Complex Models from Range Images. *Proceedings SIGGRAPH-96*, 1996, pp 303-312.

[Dodso91] Dodson, C. Poston, T., *Tensor Geometry*, Graduate Texts in Mathematics, Springer Verlag, 1991.

[Edels94] Edelsbrunner, H., Three Dimensional Alpha Shapes, *ACM Transactions on Graphics*, Vol 13, No 1, Jan , 1994, pp 43-72.

[Fomen97] Fomenko, A., Kunii, T. *Topological Modeling for Visualization*, Tokio, Springer Verlag, 1997.

[Grimm95] Grimm, C., Hughes, J., Modeling Surfaces of Arbitrary Topology using Manifolds. *Proceedings, SIGGRAPH - 95 Annual Conference Series*, Los Angeles, August 6-11, 1995, pp. 359-368.

[Guill74] Guillemin, V., Pollack, A., *Differential Topology*, New Jersey, USA, Prentice – Hall Inc., 1974.

[Golub94] Golub, V., Van Loan, A., *Matrix Computations*, Johns Hopkins Univ. Press, 1994.

[Guo97] Guo, B., Surface Reconstruction: From Points to Splines. *Computer Aided Design*, Vol 29, No 4, 1997, pp 269-277.

[Loren87] Lorensen, W., Cline, H., Marching Cubes: A High Resolution 3D Surface Construction Algorithm, *ACM Computer Graphics*, Vol. 21, No. 24, July, 1987, pp. 163-169.

[Mantÿ88] Mantÿla, M., *An Introduction to Solid Modeling*, Rockville, USA, Computer Science Press. 1988.

[McIvo97] McIvor, A., Valkenburg, R. A Comparison of Local Surface Estimation Methods. *Machine Vision and Applications*, No. 10, 1997, pp 17-26.

[Neuge97] Neugebauer P., Reconstruction of Real World Objects via Simultaneous Registration and Robust Combination of Multiple Range Images. *International Journal of Shape Modeling*, Vol. 3, No. 1&2, 1997, pp 71-90.

[O'Nei66] O'Neil, B., *Elementary Differential Geometry*, San Diego, USA, Academic Press, 1966.

[Ruiz99] Ruiz, O., Posada, J., Computational Geometry in the Preprocessing of Point Clouds for Surface Modeling. *Integrated Design and Manufacturing in Mechanical Engineering-98*. Nederlands, Kluwer Academic Publishers, 1999.

[Ruiz00] Ruiz, O., DigitLAB, an Environment and Language for Manipulation of 3D Digitizations. *Proceedings of the Joint Conference: IDMME'2000 & CSME FORUM 2000*. Montreal, Canada. May 16-19, 2000, pp 180-199.

[Stoke89] Stoker, J. J., *Differential Geometry*, Wiley – Interscience, Wiley Classics Edition, 1989.

[Turk94] Turk, G., Levoy, M., Zippered Polygon Meshed from Range Images. P*roceedings SIGGRAPH-94*, 1994, pp 311-318.

[Varad97] Varady, T., Reverse Engineering of Geometric Models – An Introduction. *Computer Aided Design*, Vol 29, No 4, 1997, pp 255-268.